Biophysical Journal, Volume *114*

Supplemental Information

Vesicle Adhesion and Fusion Studied by Small-Angle X-Ray Scattering

Karlo Komorowski, Annalena Salditt, Yihui Xu, Halenur Yavuz, Martha Brennich, Reinhard Jahn, and Tim Salditt

1 Dynamic Light Scattering

Dynamic light scattering (DLS) measurements were performed by using an ALV/CGS-3 DLS/SLS Laser Light Scattering Goniometer System (ALV GmbH Langen, Germany). The setup is equipped with a 22 mW polarized HeNe-Laser operating at a wavelength of $\lambda = 632.8$ nm (UNIPHASE, model 1145P), and an ALV-7004 Multiple Tau Digital Correlator. Scattering intensities were recorded using an ALV high quantum efficiency avalanche diode at a scattering angle of 90°. Cylindrical borosilicate cuvettes with a diameter of 10 mm (Fisher Scientific), closed with polymer caps (Carl Roth GmbH, Karlsruhe, Germany), were used as sample cells. For matching the refractive index of the cuvettes the measurement cell in the setup was filled with toluene. In all experiments the samples were diluted 1 : 500 with Milli-Q water, which was additionally filtered through a membrane of 20 nm pore size. For each sample, three runs of ten seconds were performed to calculate the intensity correlation functions. These correlation functions were than averaged to obtain the averaged intensity autocorrelation function $g_2(\tau) = \langle I(t)I(t+\tau)\rangle_t / \langle I\rangle_t^2$, which is related to the resulting normalized amplitude correlation function $g_1(\tau)$ by the Siegert relation $g_2(\tau) = 1 + \beta|g_1(\tau)|^2$ with the coherence factor β. Data analysis was performed with the ALV-Correlator Software (ALV-7004 for Windows, V.3.0.5.4) using a constrained regularization method for applying nonlinear fits to $\beta|g_1(\tau)|^2$. Fig. S1 shows size distributions of vesicles obtained by DLS for different lipid compositions with respect to the preparation step. DLS measurements were performed directly after the respective preparation step involving sonication in the first step and subsequently serial extrusion through polycarbonate membranes with pore sizes of 100, 50 and 30 nm diameter, in this order. In general, we observe that the extrusion steps affect the structure of the vesicles for both parameters, the mean radius and the polydispersity of the vesicle suspension, compared to sonicated vesicles. Both parameters are generally slightly decreased after each extrusion step. Only for DOPS huge differences can be observed for the polydispersity. Nevertheless, direct sonication of the suspension already leads to comparatively small vesicles. Note that DLS is particularly sensitive to contamination by larger aggregates, and size distribution are often 'corrected' by weighting functions, see for example (1). Here we show only unweighted distributions.

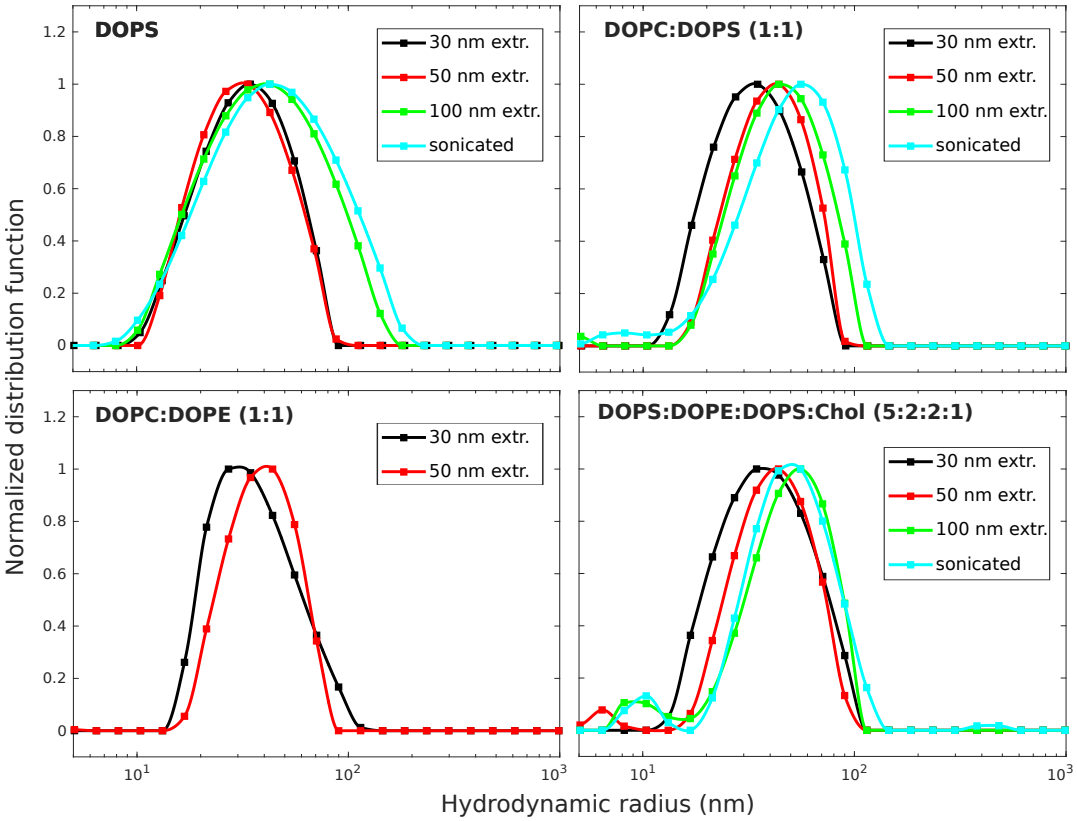

Fig. S1: Size distributions of lipid vesicles obtained by DLS for different lipid compositions with respect to the preparation step. The vesicles were first sonicated, then extruded through polycarbonate membranes with pore sizes of 100 nm, 50 nm, and 30 nm, in this order.

2 Non-interacting vesicles: additional figures and tables

Fig. S2 shows a series of SAXS profiles $I(q)$ vs q of vesicles in ultra-pure water for different lipid compositions. The measurements were performed immediately after the respective

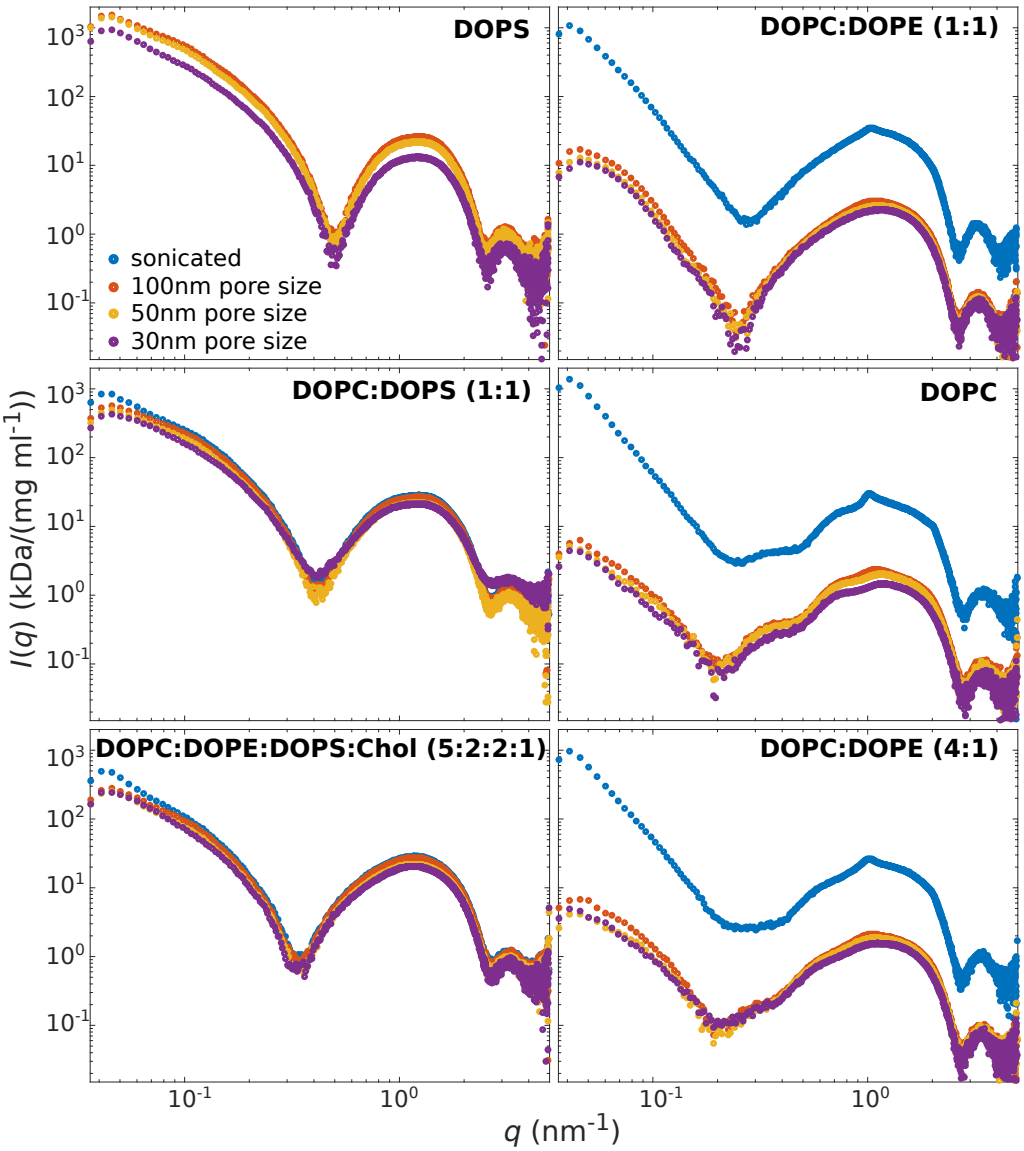

Fig. S2: SAXS data $I(q)$ vs. q for vesicles of different composition and preparation steps in ultra-pure water. The vesicles were first sonicated (blue circles), then gradually extruded through polycarbonate membranes with pore sizes of 100 nm (red circles), 50 nm (yellow circles), 30 nm (purple circles), in this order.

preparation step (subsequent extrusion through membranes of 100 nm, 50 nm and 30 nm pore size). As already discussed in the main text, we observe that vesicles containing DOPS achieve unilamellarity easily for each data set. Contrary, unilamellar vesicle using DOPC:DOPE mixtures are only achieved for DOPC:DOPE (1:1) after the final step of

extrusion through 30 nm pores.
Next, we present additional fits of non-interacting vesicles without proteins, and focus in particular on the influence of different background models. Note that the workflow always included background subtraction in form of a pure buffer measurement. However, residual errors occur if this subtraction is not completely correct for example by issues of self absorption. This can be accounted for by an additional parameterized background model (additive with either sign).

Spherical vesicle model fits with different background models. Fig. S3 shows SAXS data of (a) DOPC:DOPE (1:1)-vesicles and (b) DOPS-vesicles (black circles) as well as least-squares fits based on the spherical vesicle model (blue lines) assuming a symmetric bilayer profile. The subplots show least-squares fits for different background models: (top) Without a background model, (center) with an additional constant background model and (bottom) with an additional power-law background model (orange lines). The structural parameters and the χ^2_{red}-values obtained from the least-squares fits are summarized in Tab. S1,S2,S3.
If no background model was added to the spherical vesicle model, we observe discrepancies between the least-squares fits and the SAXS data in particular for the form factor minima. In the case of a constant background model, a good match can be observed for higher q-values, whereas discrepancies still appear in the lower q-region. The discrepancies are most pronounced for DOPC:DOPE vesicles. For DOPS vesicles the differences are less obvious, but at a closer look we observe modulations of the least-squares fit in the very low q-range which do not match with the experimental data. Using a power-law background model, we observe a good match between the least-squares fits and the data over the entire q-range. Consequently, the χ^2_{red}-values are reduced. The comparison of the two power-law backgrounds (Fig. S3, bottom) indicates that the background depends on the lipid composition of the vesicles. We conclude that the background model describes discrepancies between the SAXS data and the spherical vesicle model rather than a real effect of flawed experimental background, for example, due to deviations from a spherical structure. In the following we investigate how structural parameters depend on the background model.

Structural results for each data set, a model-based discussion. Fig. S4 displays the structural parameters for each lipid composition along with the corresponding preparation step as obtained from the least-squares analysis using the flat bilayer model with an additional constant background (blue circles), or the spherical vesicle model with either an additional constant background (green circles) or a power-law background model (red circles). The structural parameters as well as the χ^2_{red}-values can be further

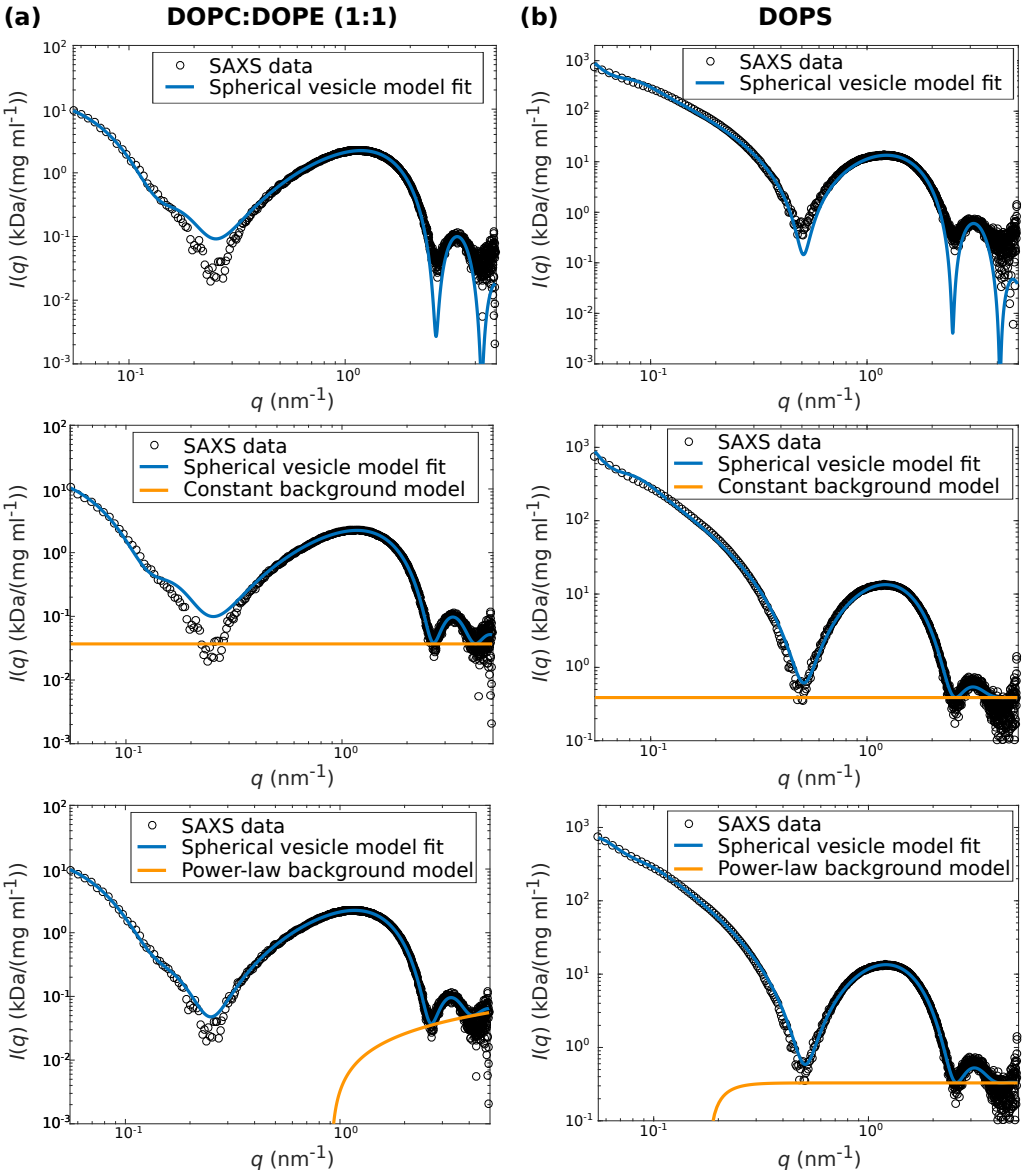

Fig. S3: Comparison of different background models (orange lines) for (a) 30nm extruded DOPC:DOPE (1:1)-vesicles and (b) 30 nm extruded DOPS-vesicles (black circles). Analysis includes spherical vesicle model least-squares fits (blue lines) without a background model (top), with a constant background model (center) and with a power-law background model (bottom).

found in the Tab. S1 (flat bilayer model, constant background), S3 (spherical vesicle model analysis, constant background) and S2 (spherical vesicle model analysis, power-law background). The four upper plots display the obtained bilayer parameters σ_{h}, σ_{c}, ρ_{h} and d_{hh}, while the two lower plots show the vesicle parameters R_0 and σ_{R}. In the case of the spherical vesicle model analysis, we observe that the obtained structural parameters depend on the underlying background model. The dependence is less pronounced for the bilayer parameters, but strong for the mean radii. By visual inspection (cf. Fig. S3), the spherical vesicle model with a constant background was not able to match the data in the lower q-region.

Comparing the results of the spherical vesicle model analysis to those of the flat bilayer model analysis, we observe that the structural bilayer parameters obtained from the flat bilayer model are systematically closer to those of the spherical vesicle model using an additional power-law background. This observation indicates that the results obtained from the spherical vesicle model with a power-law background are reasonable at least for the bilayer parameters. Still for the spherical vesicle model with a power-law background, major changes in the radius occur between vesicles extruded through 50 nm pore sizes and through 30 nm pore sizes. DOPC:DOPE (1:1)-vesicles are an exception, since for both preparation steps a radius of approximately 14 nm is obtained. Simultaneously, DOPC:DOPE (1:1)-vesicles show the smallest radius as compared to the other lipid compositions. One explanation for no or only minor changes in the radius between the preparation steps sonication and extrusion through pores of 50 nm diameter could be that already the sonication step leads to small mean radii. The mean radii obtained from the spherical vesicle model analysis with an additional constant background are significantly higher for each lipid composition. Unexpectedly, the mean radius shows an increase from the sonication step to the step of extrusion through 100 nm pores for DOPC:DOPS (1:1) and DOPC:DOPE:DOPS:Chol (5:2:2:1).

Nevertheless, independently of the background model we observe the smallest radii for DOPC:DOPE (1:1) vesicles ($\sim$ 14 to 18 nm). This observation is well in line with the fact that contrary to the other lipid compositions the net charge of the mixture is zero. Thus, there is no long-range repulsion due to a negatively charged surface. The values for the standard deviation σ_{R} of the size distribution of the vesicle suspension appear to be high with respect to the corresponding mean radius (for almost each lipid composition approximately $\sigma_{\mathrm{R}}/R_0 = 0.5$). The lowest values for σ_{R} can be found for DOPC:DOPE (1:1) vesicles.

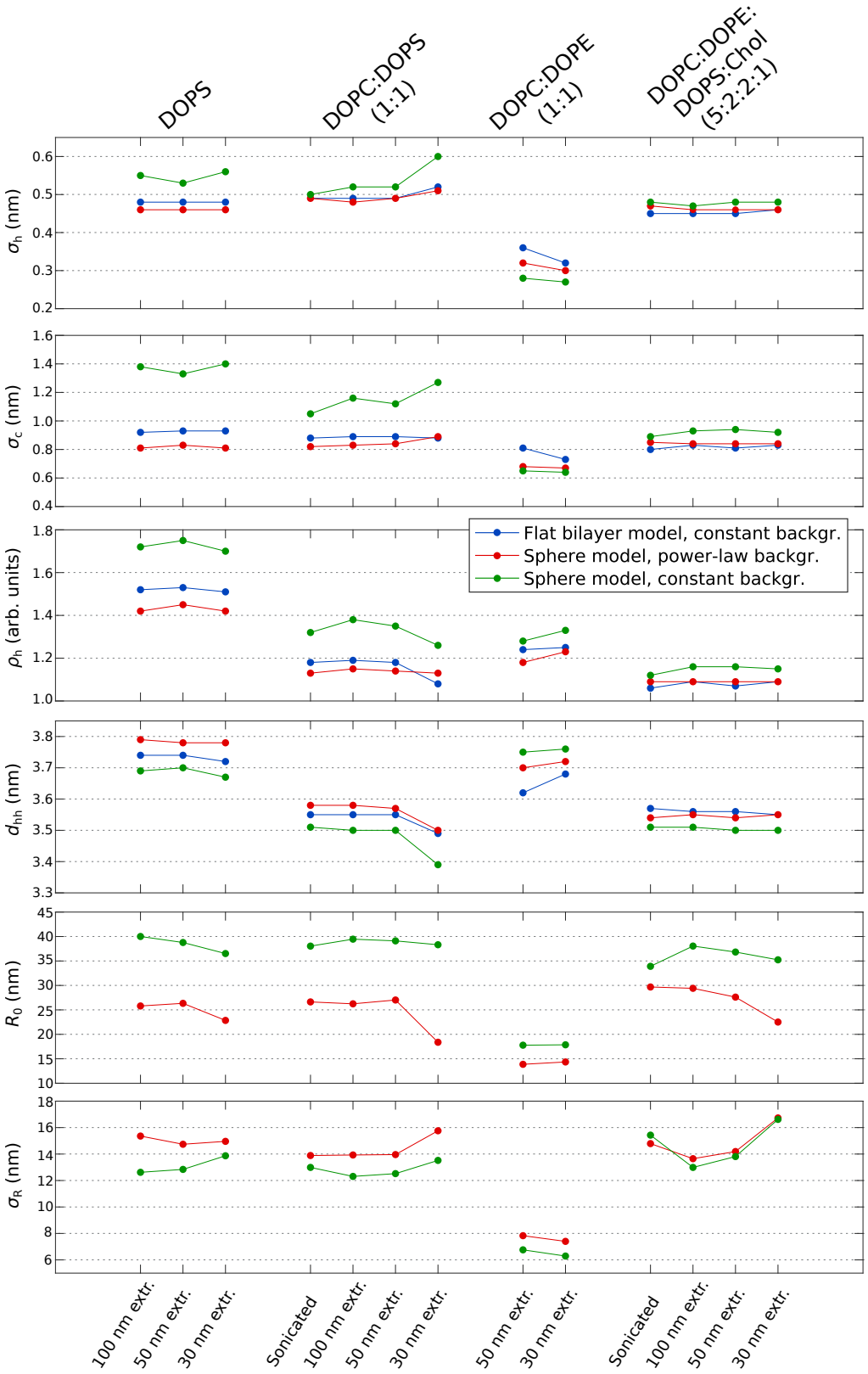

Fig. S4: Structural parameters obtained from least-squares fits using the flat bilayer model and the spherical vesicle model with different background models for 13 data sets (four different lipid compositions and up to four different preparation steps).

Lipid composition	Preparation	ρ_{h} (arb. u.)	σ_{h}, σ_{c} (nm)	d_{hh} (nm)	χ^2_{red}	c_1	c_2
DOPS	100 nm extr.	1.52	0.48, 0.92	3.74	5.19	23.34	0.64
	50 nm extr.	1.53	0.48, 0.93	3.74	3.66	19.66	0.57
	30 nm extr.	1.51	0.48, 0.93	3.72	2.30	11.92	0.35
DOPC:DOPS (1:1)	sonicated	1.18	0.49, 0.88	3.55	4.95	38.90	0.89
	100 nm extr.	1.19	0.49, 0.89	3.55	3.57	36.24	0.82
	50 nm extr.	1.18	0.49, 0.89	3.55	2.67	30.36	0.68
	30 nm extr.	1.08	0.52, 0.88	3.49	3.94	31.31	1.45
DOPC:DOPE (1:1)	50 nm extr.	1.24	0.36, 0.81	3.62	2.79	3.87	0.05
	30 nm extr.	1.26	0.32, 0.73	3.68	1.15	3.56	0.04
DOPC:DOPE:DOPS:Chol (5:2:2:1)	sonicated	1.06	0.45, 0.80	3.57	2.00	43.47	0.78
	100 nm extr.	1.09	0.45, 0.83	3.56	1.73	40.79	0.73
	50 nm extr.	1.07	0.45, 0.81	3.56	1.72	33.57	0.61
	30 nm extr.	1.09	0.46, 0.83	3.55	1.73	30.88	0.55

Tab. S1: Structural parameters obtained from flat bilayer model fits to SAXS data of various lipid compositions with respect to the preparation (sonicated and extruded through polycarbonate membranes with pore sizes 100 nm, 50 nm and 30 nm in diameter). The model fits are based on a symmetric electron density profile, thus the amplitude and width of the inner and outer leaflet are $\rho_{\mathrm{h}} = \rho_{\mathrm{h1}} = \rho_{\mathrm{h2}}$ and $\sigma_{\mathrm{h}} = \sigma_{\mathrm{h1}} = \sigma_{\mathrm{h2}}$. The amplitude of the Gaussian representing the chain region is selected to $\rho_c = -1$ (arb. units) for all fits.

Lipid composition	Preparation	ρ_{h} (arb. u.)	σ_{h}, σ_{c} (nm)	d_{hh} (nm)	R_0 (nm)	σ_R (nm)	χ^2_{red}	c_1	c_2	c_3	c_4
DOPS	100 nm extr.	1.42	0.46, 0.81	3.79	25.8	15.36	9.14	0.014	$-7.42 \cdot 10^{-6}$	6.52	0.61
	50 nm extr.	1.45	0.46, 0.83	3.78	26.34	14.74	5.92	0.011	$-2.93 \cdot 10^{-6}$	6.77	0.54
	30 nm extr.	1.42	0.47, 0.81	3.78	22.85	14.96	3.77	0.008	$-5.15 \cdot 10^{-6}$	6.42	0.33
DOPC:DOPS (1:1)	sonicated	1.13	0.49, 0.82	3.58	26.63	13.89	7.56	0.022	$-2.54 \cdot 10^{-7}$	7.43	0.86
	100 nm extr.	1.15	0.48, 0.83	3.58	26.24	13.93	5.61	0.021	$-1.36 \cdot 10^{-6}$	6.88	0.79
	50 nm extr.	1.14	0.49, 0.84	3.57	27.02	13.96	3.63	0.017	$-3.24 \cdot 10^{-7}$	7.28	0.65
	30 nm extr.	1.13	0.51, 0.89	3.5	18.38	15.76	3.79	0.026	$-2.52 \cdot 10^{-5}$	5.8	1.41
DOPC:DOPE (1:1)	50 nm extr.	1.18	0.32, 0.68	3.7	13.87	7.83	3.34	0.009	1010.85	$-3.97 \cdot 10^{-5}$	-1010.85
	30 nm extr.	1.23	0.3, 0.67	3.72	14.35	7.4	1.42	0.007	808.51	$-4.05 \cdot 10^{-5}$	-808.51
DOPC:DOPE:DOPS:Chol (5:2:2:1)	sonicated	1.09	0.47, 0.85	3.54	29.68	14.79	3.05	0.021	$-3.04 \cdot 10^{-12}$	10.77	0.76
	100 nm extr.	1.09	0.46, 0.84	3.55	29.41	13.65	2.47	0.020	$-9.71 \cdot 10^{-10}$	8.96	0.71
	50 nm extr.	1.09	0.46, 0.84	3.54	27.61	14.19	2.1	0.018	$-8.22 \cdot 10^{-10}$	8.93	0.59
	30 nm extr.	1.09	0.46, 0.84	3.55	22.51	16.73	2.08	0.019	$-1.97 \cdot 10^{-10}$	9.34	0.53

Tab. S2: Structural parameters obtained from spherical vesicle model fits $I_{\mathrm{tot}}(q) = c_1 I_{\mathrm{sphere}}(q) + c_2 q^{-c_3} + c_4$ to SAXS data of various lipid compositions with respect to the preparation (sonicated and extruded through polycarbonate membranes with pore sizes 100 nm, 50 nm and 30 nm in diameter). The model fits are based on a symmetric electron density profile, thus the amplitude and width of the inner and outer leaflet are $\rho_{\mathrm{h}} = \rho_{\mathrm{h1}} = \rho_{\mathrm{h2}}$ and $\sigma_{\mathrm{h}} = \sigma_{\mathrm{h1}} = \sigma_{\mathrm{h2}}$. The amplitude of the Gaussian representing the chain region is selected to $\rho_c = -1$ (arb. units) for all fits.

Lipid composition	Preparation	ρ_{h} (arb. u.)	σ_{h}, σ_{c} (nm)	d_{hh} nm)	R_0 (nm)	σ_R (nm)	χ^2_{red}	c_1	c_2
DOPS	100 nm extr.	1.72	0.55, 1.38	3.69	40.01	12.62	58.38	0.004	0.39
	50 nm extr.	1.75	0.53, 1.33	3.70	38.78	12.84	34.58	0.006	0.60
	30 nm extr.	1.70	0.56, 1.40	3.67	36.52	13.87	21.58	0.007	0.71
DOPC:DOPS (1:1)	sonicated	1.32	0.50, 1.05	3.51	38.04	12.99	22.37	0.012	0.88
	100 nm extr.	1.38	0.52, 1.16	3.50	39.46	12.31	26.72	0.010	0.84
	50 nm extr.	1.35	0.52, 1.12	3.50	39.11	12.52	15.89	0.009	0.68
	30 nm extr.	1.26	0.60, 1.27	3.39	38.32	13.52	15.25	0.011	1.48
DOPC:DOPE (1:1)	50 nm extr.	1.28	0.28, 0.65	3.75	17.78	6.76	4.89	0.006	0.04
	30 nm extr.	1.33	0.27, 0.64	3.76	17.86	6.29	2.39	0.005	0.04
DOPC:DOPE:DOPS:Chol (5:2:2:1)	sonicated	1.12	0.48, 0.89	3.51	33.91	15.43	3.42	0.015	0.77
	100 nm extr.	1.16	0.47, 0.93	3.51	38.05	12.99	4.65	0.012	0.72
	50 nm extr.	1.16	0.48, 0.94	3.50	36.83	13.81	3.44	0.010	0.60
	30 nm extr.	1.15	0.48, 0.92	3.50	35.24	16.62	2.52	0.010	0.54

Tab. S3: Constant Background. Structural parameters obtained from spherical vesicle model fits to SAXS data of various lipid compositions with respect to the preparation (sonicated and extruded through polycarbonate membranes with pore sizes 100 nm, 50 nm and 30 nm in diameter). The model fits are based on a symmetric electron density profile, thus the amplitude and width of the inner and outer leaflet are $\rho_{\mathrm{h}} = \rho_{\mathrm{h1}} = \rho_{\mathrm{h2}}$ and $\sigma_{\mathrm{h}} = \sigma_{\mathrm{h1}} = \sigma_{\mathrm{h2}}$. The amplitude of the Gaussian representing the chain region is selected to $\rho_c = -1$ (arb. units) for all fits.

3 Adhesion of vesicles: additional figures and tables

Based on the analysis of the SAXS data of $CaCl_2$- and $MgCl_2$-induced adhesion of lipid vesicles presented in the main manuscript (Fig. 5, Tab. 2), we further compare the EDPs upon addition of the divalent ions and of the control (without divalent ions) in Fig. S5. Both for $CaCl_2$ and $MgCl_2$ a swelling of the lipid bilayer is observed. Subtraction of the EDPs ($\rho_{CaCl_2} - \rho_{control}$ and $\rho_{MgCl_2} - \rho_{control}$) gives pronounced peaks close to the headgroup maxima (identified as the phosphorus), revealing the position of the condensated Ca^{2+} and Mg^{2+} ions. Accordingly, the ions are located near the bilayer surface with a rather small penetration depth into the headgroup region (the insertion is less for Ca^{2+}).

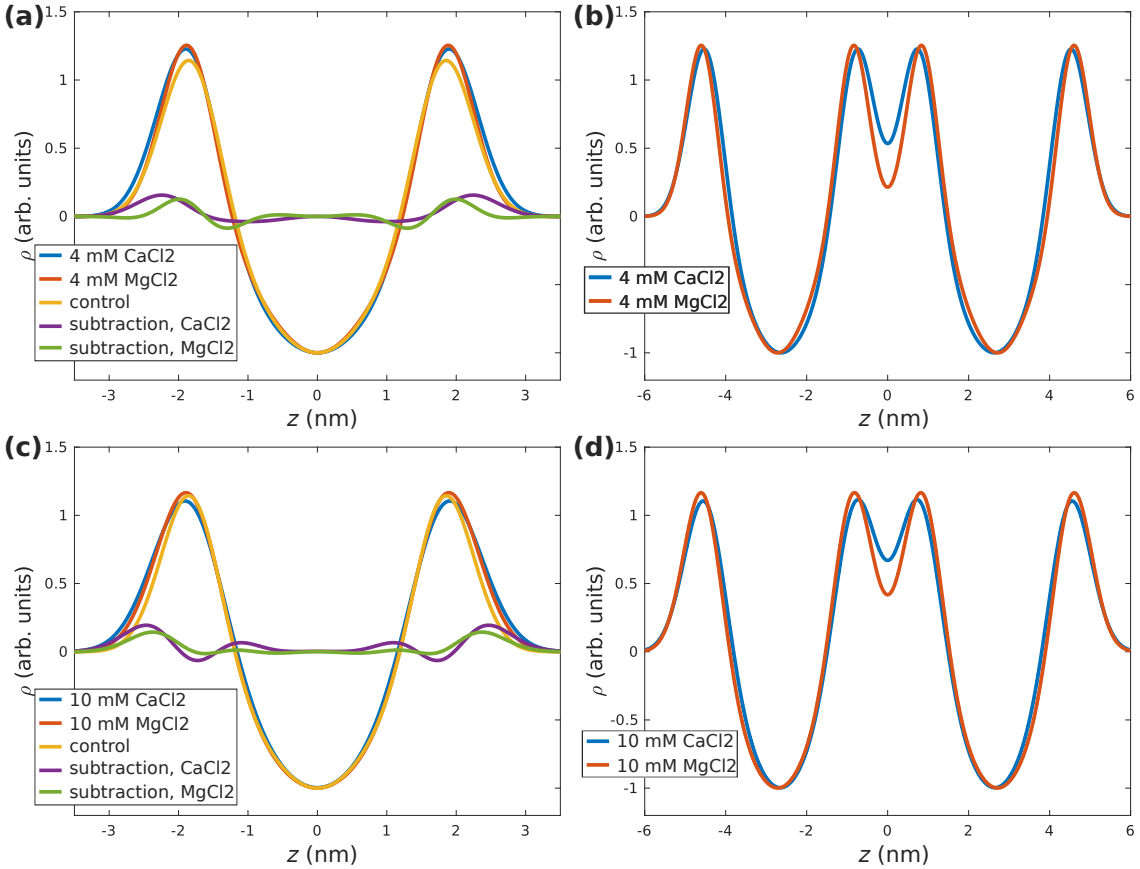

Fig. S5: Reconstructed EDPs of DOPC:DOPS (1:1) with (a,b) 4 mM $CaCl_2$/$MgCl_2$ and (c,d) 10 mM $CaCl_2$/$MgCl_2$ using the structural parameters obtained from the flat bilayer model fits and from the docking model fits presented in the main manuscript in Fig. 5 and Tab. 2. The EDPs indicated as control correspond to the flat bilayer analysis of the SAXS data without added salts.

Next, we present data obtained in a soft adhesion regime with inter-bilayer water distances much larger than for the strong adhesion regime described in the main manuscript. This regime is observed when the addition of $CaCl_2$ is accompanied by monovalent salt (KCl).

For the recording of that data, we have used $CaCl_2$ in a HEPES buffer (10mM $CaCl_2$, 150mM KCl and 20mM Hepes, pH 7.4). Fig. S6 shows the corresponding series of SAXS curves $I(q)$ vs. q of vesicles initially suspended in ultra-pure water, as a function of the added $CaCl_2$ and KCl concentration. The SAXS profiles of the DOPC:DOPS (1:1) mixture

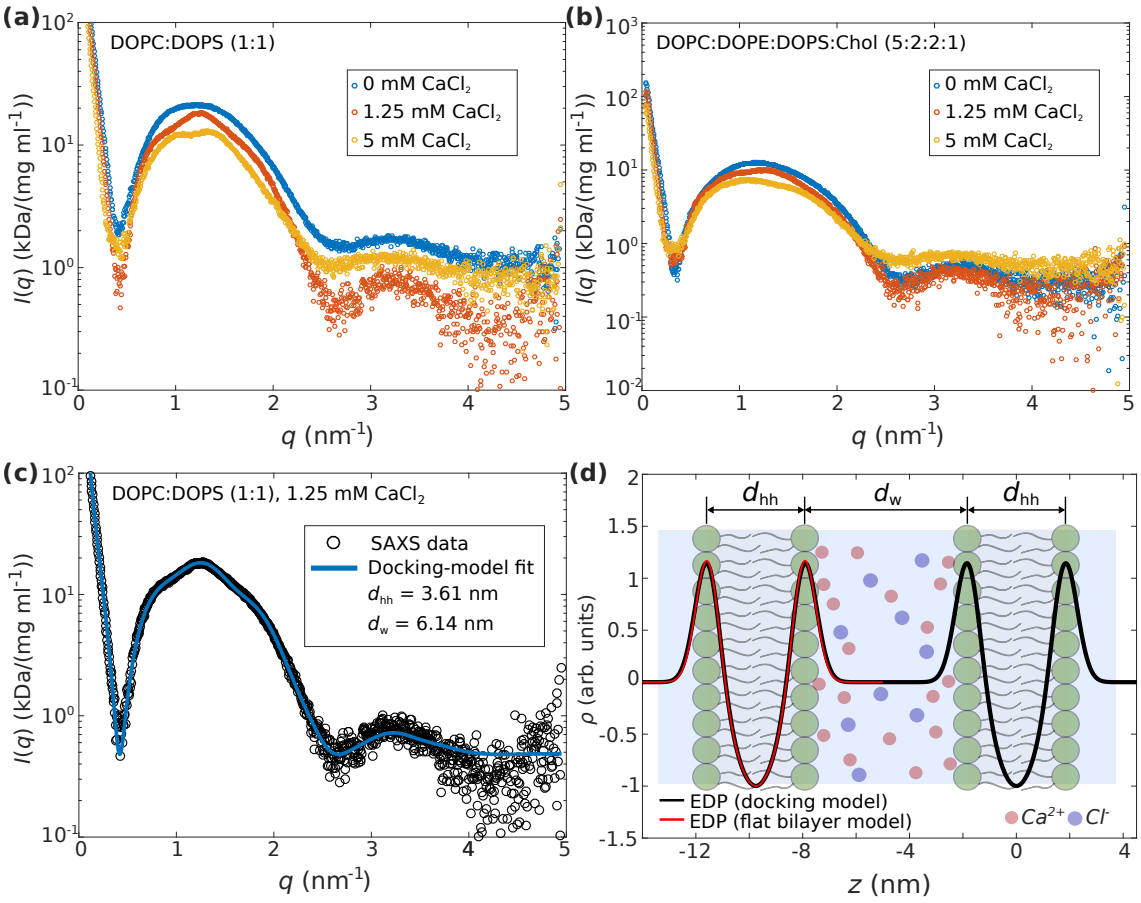

Fig. S6: (a) SAXS data of DOPC:DOPS (1:1) vesicles in Milli-Q water with added $CaCl_2$ with concentrations of 0 mM (blue), 1.25 mM (red) and 5 mM (yellow). (b) SAXS data of DOPC:DOPE:DOPS:Chol (5:2:2:1) vesicles in Milli-Q water with added $CaCl_2$ with concentrations of 0 mM (blue), 1.25 mM (red) and 5 mM (yellow). (c) Scattering curve as obtained from DOPC:DOPS (1:1) vesicles in Milli-Q water upon addition of 1.25 mM $CaCl_2$ (black circles) and least-squares fit using the docking model (blue line). (d) EDP as obtained from the docking model fit indicated in (c). The structural parameters are summarized in Tab. S4.

(a) and the DOPC:DOPE:DOPS:Chol (5:2:2:1) mixture (b) show the characteristic structure factor modulations of two membranes in an adhering state. The modulation varying systematically with ion concentrations, indicating that the range of water layer spacings is much more variable than in the strong adhesion regime. As an example, we explicitly show in (c) the analysis of the SAXS data of DOPC:DOPS (1:1) vesicles in the presence of 1.25 mM $CaCl_2$ and 18.75 mM KCl, based on the docking model with a constant background

model. The structural parameters obtained from the least-squares fits to the docking model are listed in Tab. S4 for each data set. In (d), the corresponding EDP of the two docked bilayers is displayed (black line). Next to the structural bilayer parameters, the interbilayer spacing (or water spacing) is quantified in a robust manner, yielding $d_{\mathrm{w}} = 6.14$ nm. Furthermore, the EDP of unilamellar DOPC:DOPS (1:1) vesicles as obtained from the flat bilayer model fit (supplementary information, Tab. 1) is indicated (red line). In this example, the bilayer structure exhibits only minor changes due to the addition of $CaCl_2$. As is apparent from Tab. S4, the water spacing is decreased for an increased $CaCl_2$ concentration ($d_{\mathrm{w}} = 3.79$ nm in the case of 5 mM $CaCl_2$). For the more complex lipid mixture of DOPC:DOPE:DOPS:Chol (5:2:2:1), a similar trend can be observed. While the water spacing of $d_{\mathrm{w}} = 5.48$ nm is again rather high for 1.25 mM $CaCl_2$, a decreased water spacing of $d_{\mathrm{w}} = 3.03$ was obtained for 5 mM $CaCl_2$. Interestingly, comparing the values for d_{w} between the different lipid compositions at the same $CaCl_2$ concentration, we can see that the water spacing is always smaller for DOPC:DOPE:DOPS:Chol (5:2:2:1). This observation may result from the lower surface charge density σ in the 4-component mixture (20 mol% DOPS).

In summary, we observe the following: (1) An increase of the $CaCl_2$ and KCl concentration yields a decrease of the interbilayer spacing d_{w} and (2) an increase of σ at constant ion concentrations yields an increase of d_{w}.

Lipid composition	[$CaCl_2$] (mM)	[KCl] (mM)	ρ_{h} (a. u.)	σ_{h}, σ_{c} (nm)	d_{hh} (nm)	d_{w} (nm)	$(1-\nu_{\mathrm{d}})$	χ^2_{red}
DOPC:DOPS (1:1)	1.25	18.75	1.27	0.46, 089	3.61	6.14	0.96	1.7
	5	75	1.32	0.38, 0.75	3.79	4.82	0.97	2.2
DOPC:DOPE:DOPS:Chol (5:2:2:1)	1.25	18.75	1.09	0.46, 0.85	3.6	5.48	0.98	2.26
	5	75	1.02	0.47, 0.83	3.58	3.69	0.97	1.39

Tab. S4: Structural parameters as obtained from docking model fits to SAXS data of docked DOPC:DOPS (1:1) and DOPC:DOPE:DOPS:Chol (5:2:2:1) vesicles with respect to the $CaCl_2$ concentration. The model fits are based on a symmetric EDP, thus the amplitude and width of the inner and outer leaflet are $\rho_{\mathrm{h}} = \rho_{\mathrm{h1}} = \rho_{\mathrm{h2}}$ and $\sigma_{\mathrm{h}} = \sigma_{\mathrm{h1}} = \sigma_{\mathrm{h2}}$. The amplitude of the Gaussian representing the chain region is selected to $\rho_c = -1$ for all fits.

4 SNARE-mediated liposome fusion and docking experiments

To study SNARE-mediated liposome fusion intermediates, two types of experiments were performed. For the docking and fusion experiments liposomes reconstituted with either the mutant SybΔ84, or with SybWT, respectively, were used. For both experiments liposomes reconstituted with the ΔN complex as the acceptor complex were used. Fusion is distinctly inhibited by using the SybΔ84 mutant (2).

In (a) and (b) the SAXS curves $I(q)$ vs. q are shown for the fusion experiment (mixed SybWT- and ΔN-liposomes at a molar ratio of 1:1) and the docking experiments (mixed SybΔ84- and ΔN-liposomes at a molar ratio of 1:1), respectively. Furthermore, the SAXS data of the docking and fusion experiments are compared to the mean scattering of the individual SNARE-liposomes. The mean scattering curve would be the expected scattering curve if no reaction occurred upon mixing. Then the scattering intensity is the incoherent superposition $I(q) = (I_{\mathrm{A}}(q) + I_{\mathrm{B}}(q))/2$ of the two individual contributions. The factor $1/2$ accounts for the dilution of each individual SNARE-liposome population. By comparison of the mean scattering curves and the scattering curves from the docking and fusion experiments, we observe small but systematic differences in the low q-region, and a slight increase of the scattering intensity over the entire q-region.

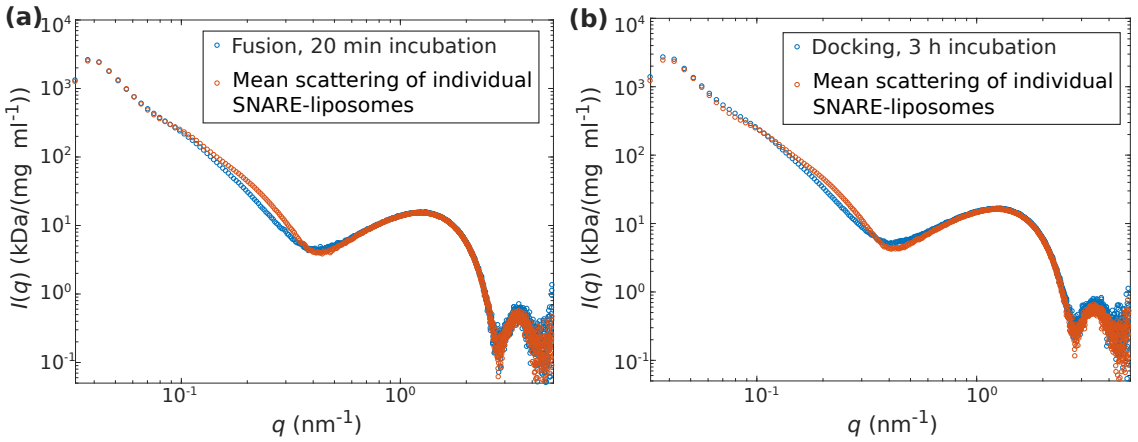

Fig. S7: (a) and (b) show SAXS data of SNARE-mediated fusion (mixed SybWT- and ΔN-liposomes) and docking (mixed SybΔ84- and ΔN-liposomes) experiments compared to the calculated mean scattering curves $(I_{\mathrm{SybWT}}(q) + I_{\Delta\mathrm{N}}(q))/2$ in the case of the fusion experiments and $(I_{\mathrm{SybΔ84}}(q) + I_{\Delta\mathrm{N}}(q))/2$ in the case of the docking experiment

In the case of the docking experiments, the characteristic structure factor modulations observed in the calcium-induced vesicle adhesion are not observed. Therefore, it is not possible to analyze the SAXS data by least-squares fits using the docking model to obtain the water spacing d_{w}. We conclude that the signal of the docking and fusion states may

have been lost in the ensemble average of the SAXS experiment, i.e.that docking and fusion efficiencies have been insufficient. This conclusion is supported by the following estimate of the increase of the forward scattering intensity, made for the case of 100 % fusion efficiency, we consider a form factor model of a spherical shell. The scattering intensity $I_{\mathrm{shell}}(q)$ is given by (3)

$$\begin{aligned} I_{shell}(q) &= \Delta\rho^2 V_{\mathrm{shell}}^2 |f_{\mathrm{shell}}(q)|^2 \\ &= \Delta\rho^2 V_{\mathrm{shell}}^2 \left| \frac{V(R_{\mathrm{out}}) f_{\mathrm{sphere}}(q, R_{\mathrm{out}}) - V(R_{\mathrm{in}}) f_{\mathrm{sphere}}(q, R_{\mathrm{in}})}{V(R_{\mathrm{out}}) - V(R_{\mathrm{in}})} \right|^2 , \end{aligned} \tag{1}$$

where

$$f_{\mathrm{sphere}}(q, R) = \frac{3(\sin(qR) - qR\cos(qR))}{(qR)^3} \tag{2}$$

is the form factor of a homogeneous sphere, $V(R) = 4/3\pi R^3$ is the volume of a sphere with the radius R, and $V_{\mathrm{shell}} = 4/3\pi(R_{\mathrm{out}}^3 - R_{\mathrm{in}}^3)$ is the volume of the shell with the outer and inner radius R_{out} and R_{in}, respectively. For the forward scattering intensity $q \to 0$ the form factor of the spherical shell becomes $f_{\mathrm{shell}} \approx 1$, so that

$$I_{\mathrm{shell}}(0) \propto V_{\mathrm{shell}}^2 \propto \left(R_{\mathrm{out}}^3 - R_{\mathrm{in}}^3 \right)^2 . \tag{3}$$

For example, if we consider an outer radius of $R_{\mathrm{out}} = 40$ nm and an inner radius $R_{\mathrm{in}} = 35$ nm in the original state, then the radii of fused spherical shells are approximately $R_{\mathrm{out}} = 50$ nm and $R_{\mathrm{in}} = 45$ nm by assuming that the volume of the two spherical shells remain after fusion, that means $V_{\mathrm{fused}} = 2V$ and thus $R_{\mathrm{fused}} = 2^{1/3}R$. This assumption yields an increase of $\sim 56\%$ of the forward scattering intensity, which is far away from the experimental observations. Altogether, the results indicate that some reactions occurred, but we can not clearly distinguish between a docked and a fused state, most likely, due to a very low efficiency of the reactions.

Supporting References

1. Castorph, S., S. Schwarz Henriques, M. Holt, D. Riedel, R. Jahn, and T. Salditt. 2011. Synaptic vesicles studied by dynamic light scattering. *Eur. Phys. J. E.* 34:1–11.

2. Hernandez, J. M., A. Stein, E. Behrmann, D. Riedel, A. Cypionka, Z. Farsi, P. J. Walla, S. Raunser, and R. Jahn. 2004. Membrane Fusion Intermediates via Directional and Full Assembly of the SNARE Complex. *Science.* 336:1581–1584.

3. Als-Nielsen, J., and D. McMorrow. 2011. Bibliography, in Elements of Modern X-ray Physics, Second Edition. John Wiley & Sons, Inc. Hoboken, NJ, USA.